

# Non-Abelian self-organized criticality model with one stochastic site in each avalanche shows multifractal scaling

Jozef Černák

*Institute of Physics, P. J. Šafárik University in Košice, Jesenn 5, Košice, Slovak Republic*

## Abstract

I have proposed a *non-Abelian* and stochastic self-organized criticality model in which each avalanche contains one stochastic site and all remaining sites in the avalanche are deterministic with a constant threshold  $E_c^I$ . Studies of avalanche structures, waves and autocorrelations, size moments and probability distribution functions of avalanche size, for the thresholds  $4 \leq E_c^I \leq 256$ , were performed. The shell-like avalanche structures, correlated waves within avalanches, complex size moments and probability distribution functions show multifractal scaling like the *Abelian* and deterministic BTW model despite the fact that the model is *non-Abelian* and stochastic with unbalanced relaxation rules at each stochastic site.

PACS numbers: 45.70.Ht, 05.65.+b, 05.70.Jk, 64.60.Ak

## I. INTRODUCTION

Bak, Tang, and Wiesenfeld (BTW) [1] introduced a concept of self-organized criticality (SOC) to study dynamical systems with temporal and spatial degrees of freedom. They designed a simple cellular automaton with conservative and deterministic relaxation rules to demonstrate the SOC phenomenon. Manna (M) [2] proposed another conservative SOC model in which stochastic relaxation rules instead of deterministic rules were defined.

A stable configuration (see below) in the BTW model does not depend on the order of relaxations so the model is Abelian [3]. On the other hand, a stable configuration in the M model depends on the order of relaxations and the model is thus non-Abelian. Dhar [4] theoretically proved the Abelian property of the M model for the case when probabilities of many final stable configurations are considered.

Based on the real-space renormalization group calculations, Pietronero *at al.* [5] claimed that both deterministic [1] and stochastic [2] models belong to the same universality class, i.e. a small modification in the relaxation rules of the models cannot change the universality class. It was assumed that both models show a finite size scaling (FSS) [6]. With FSS the avalanche size, area, lifetime, and perimeter follow power laws with cutoffs [6]:

$$P(x) = x^{-\tau_x} F(x/L^{D_x}), \quad (1)$$

where  $P(x)$  is the probability density function of  $x$ ,  $F$  is the cutoff function, and  $\tau_x$  and  $D_x$  are the scaling exponents. The set of scaling exponents  $(\tau_x, D_x)$  defines the universality class [6].

Avalanche structure studies [7] and numerical simulations [8] showed that the BTW and M models do not belong to the same universality class. Later, Tebaldi *at al.* [9] found that avalanche size distributions in the BTW model follow multifractal scaling. They concluded that the avalanche size exponent  $\tau_s$  (Eq. 1) does not apply to the BTW model. An avalanche wave decomposition approach [10] was applied [11] to demonstrate the different wave features of the BTW and M models. Karmakar *at al.* [12] found that models with balanced relaxation rules are similar to the deterministic BTW model and models with unbalanced relaxation rules are similar to stochastic M-like models. These results [7–9, 11, 12] support the idea that the BTW and Manna models are prototypes of different universality classes.

The BTW and M models are well understood [3, 4, 7–9]. On the hand, we know very little

about the transition from multifractal to fractal scaling [12, 13]. I modified the BTW model [1] to study this transition. I allowed stochastic relaxations in one site in each avalanche. The stochastic site is located in the place where the avalanche is initiated. Avalanches are randomly initiated in various lattice sites so the position of stochastic site is changed at every new avalanche and the stochastic M-like site can visit all lattice sites for sufficiently large set of avalanches. An avalanche dynamics study [11] is useful to understand the transition from multifractal to fractal scaling and to test the hypothesis of precise relaxation balance [12]. The results suggest that the model cannot belong to either BTW or M universality classes.

In Sec. II I introduce a *non-Abelian* and stochastic model. In Sec. III I apply numerical simulations and statistical methods to find avalanche structures, autocorrelation functions, Hurst exponents, avalanche size moments and probability density functions of avalanche sizes. Section IV is devoted to a discussion which is followed by conclusions in Sec. V.

## II. STOCHASTIC SELF-ORGANIZED CRITICALITY MODEL

The stochastic SOC model is defined on a two dimensional (2D) lattice  $L \times L$  where each site  $\mathbf{i}$  has assigned two dynamical variables  $E(\mathbf{i})$  and  $E_c(\mathbf{i})$  [13]. The variable  $E(\mathbf{i})$  represents for example, energy and variable  $E_c(\mathbf{i})$  represents a threshold at site  $\mathbf{i}$ . All thresholds  $E_c(\mathbf{i})$  are equal to the same value  $E_c^I$  in the interval  $4 \leq E_c^I \leq 256$ . Relaxation rules are undirected, conservative and deterministic for all sites  $\mathbf{i}$  with the thresholds  $E_c(\mathbf{i}) = E_c^I$ . At each site  $\mathbf{i}$  the relaxation rules are precisely balanced [12]. Thus the sites behave as the BTW sites [1] for the threshold  $E_c^I = 4$ . In a stable configuration (a stationary state), all sites  $\mathbf{i}$  follow  $E(\mathbf{i}) < E_c(\mathbf{i})$ . Let us assume that from a stable configuration we iteratively select  $\mathbf{i}$  at random and increase  $E(\mathbf{i}) \rightarrow E(\mathbf{i}) + 1$ . If an unstable configuration is reached, i.e.  $E(\mathbf{i}) \geq E_c^I$ , then the site  $\mathbf{i}$  is labeled as  $\mathbf{i}_M$ . The initial threshold at site  $\mathbf{i}_M$ ,  $E_c(\mathbf{i}_M) = E_c^I$  is changed to the new value  $E_c(\mathbf{i}_M) = E_c^{II} = 2$  and stochastic relaxation rules [2] are assigned to this site. In each avalanche only one site  $\mathbf{i}_M$  undergoes stochastic relaxations while all remaining sites relax as undirected, deterministic and conservative sites. All unstable sites  $\mathbf{i}$  (including  $\mathbf{i}_M$ ) where  $E(\mathbf{i}) \geq E_c(\mathbf{i})$  undergo relaxations to reach the stable configuration  $E(\mathbf{i}) < E_c(\mathbf{i})$ . If a stable configuration is reached, then the threshold  $E_c(\mathbf{i}_M)$  at the site  $\mathbf{i}_M$  is set to  $E_c(\mathbf{i}_M) = E_c^I$  and deterministic relaxation rules [1] are assigned to the site  $\mathbf{i}_M$ . The site  $\mathbf{i}_M$  disappears and

all sites  $\mathbf{i}$  of the lattice are BTW-like sites. Stable and unstable states are repeated many times. Adding of energy ( $E(\mathbf{i}) \rightarrow E(\mathbf{i}) + 1$ ) takes place randomly thus stochastic sites  $\mathbf{i}_M$  could visit all lattice sites. Thus stochastic sites introduce an annealed disorder in the initial deterministic model [1].

### III. RESULTS

One stochastic site in each avalanche makes the model stochastic [14].

All sites, except one, relax energy as *Abelian* sites [3, 15], however I classified the model as non-Abelian. To demonstrate the *non-Abelian* property consider two critical sites [15] (Fig. 1) with thresholds  $E_c^{II} = 2$  (the stochastic site) and  $E_c^I = 4$  (the deterministic site). One can verify (Fig. 1) that the order of relaxations of unstable sites leads to different final stable configurations i.e. the OSS model is *non-Abelian*.

Relaxations in all deterministic sites are precisely balanced [12]. However, one site in each avalanche shows unbalanced relaxations. Thus we consider the OSS model for the model with unbalanced relaxation rules.

Analyzing the avalanche structures can provide an important initial information [7, 12, 16] about the nature of the SOC model. Several avalanches of the OSS model, at the threshold  $E_c^I = 4$ , have been decomposed into clusters with equal numbers of relaxations (Fig. 2). Avalanche structures of two types: (i) without holes Fig. 2(a) and (ii) with rare holes in clusters Fig. 2(b) were observed. These structures are similar to shell-like structures one finds in the BTW model.

The study of mathematical SOC models allows avalanches to be decomposed avalanches into waves [10]. This approach enables the investigation of correlation of waves within the avalanche [11]. I demonstrated that the OSS model is *non-Abelian*, thus the avalanche waves could be defined as in the case of the M model [11]. On the other hand, waves initiated by relaxations of the stochastic site ( $\mathbf{i}_M$ ) propagate though the lattice of BTW sites. Thus waves would be defined as well as waves of the BTW model. An avalanche of size  $s$  is decomposed into  $m$  waves with sizes  $s_k$ , where  $s = \sum_{k=1}^m s_k$ . A time-sequence of avalanche waves  $s_k$  is used to determine the autocorrelation function [11, 17]

$$C(t, L) = \frac{\langle s_{k+t} s_k \rangle_L - \langle s_k \rangle_L^2}{\langle s_k^2 \rangle_L - \langle s_k \rangle_L^2}, \quad (2)$$

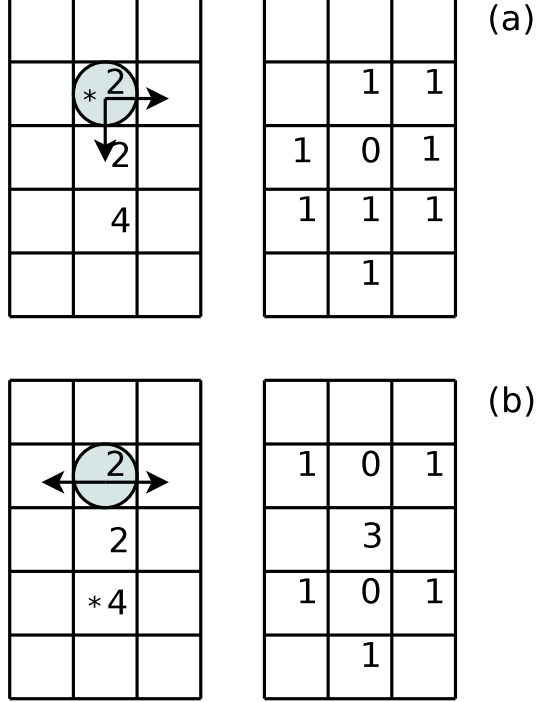


FIG. 1: (color online) Order of relaxations of the critical sites shows the *non-Abelian* property of the OSS model. The circle denotes a stochastic site and the star (\*) denotes a site which relaxes as first. In the initial state there are two critical sites  $E_c^{II} = 2$  (stochastic) and  $E_c^I = 4$ . (a) The stable configuration in the case when the stochastic site ( $E_c^{II} = 2$ ) relaxed as first. (b) The stable configuration in the case when the deterministic site ( $E_c^I = 4$ ) relaxed as first. Arrows show directions of energy diffusion in the stochastic site.

where time is  $t = 1, 2, \dots$ , and the time averages are taken over  $5 \times 10^6$  waves for lattice sizes  $L = 128, 256, 512, 1024, 2048$  and  $4096$ . The autocorrelations  $C^{BTW}(t, L)$  of the BTW model (Fig. 3(a)) and  $C^{OSS}(t, L)$  of the OSS model at threshold  $E_c^I = 4$  (Fig. 3(b)) approach zero only for times  $t_{max}^{BTW}$  and  $t_{max}^{OSS}$  exceeding the maximum number of waves in avalanches. This result is a consequence of correlated waves in avalanches [11]. I have observed (Fig. 3) that at a given lattice size  $L$ , the time  $t_{max}^{OSS}$  is approximately as large as time  $t_{max}^{BTW}$  ( $t_{max}^{OSS} \doteq t_{max}^{BTW}$ ). I note that avalanche waves in the M model are uncorrelated due to autocorrelation functions  $C^M(t, L) \doteq 0$  for  $t \geq 1$  [11, 12].

The autocorrelations  $C^{BTW}(t, L)$  (Eq. 2) of the BTW model were approximated by a power law  $f(t) \sim t^{-\tau_c}$  and cutoff function  $g(t/L^{D_c})$  [11]:

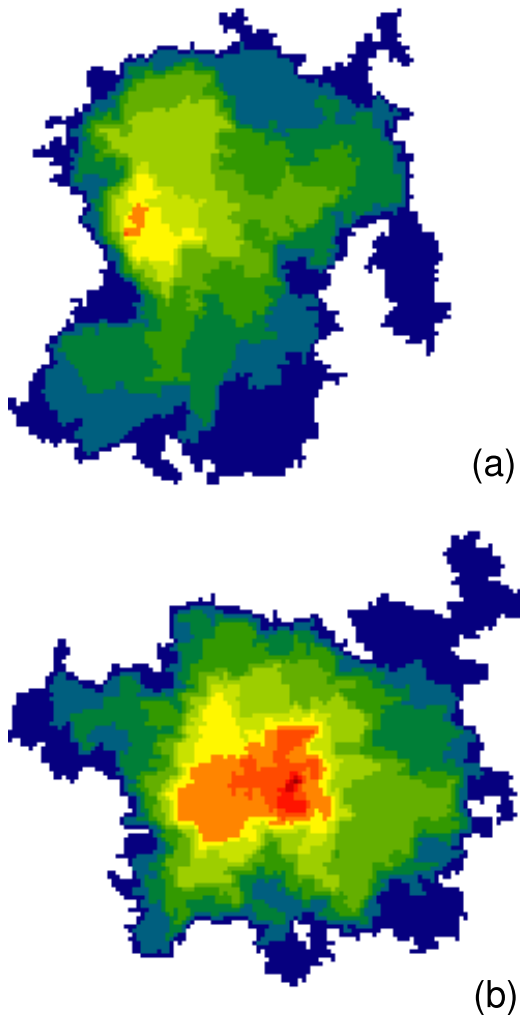


FIG. 2: (color online) Two types of avalanche structures on a 2D lattice of size  $128 \times 128$ : (a) without holes in the clusters and (b) with holes in clusters. Lattice sites with the same numbers of relaxations are shown by the same color (rainbow pseudo-color coding). Only one site in any avalanche relaxes in a stochastic manner as a M site (the red area), however all remaining sites relax in a deterministic manner as BTW sites ( $E_c^I = 4$ ).

$$C^{BTW}(t, L) = f(t)g(t/L^{D_c}). \quad (3)$$

The autocorrelations  $C^{BTW}(t, L)$  (Fig. 3(a)) agree well with the previous results [11, 12]. However, I have found that the power law approximation  $f(t) \sim t^{-\tau_c}$  does not approximate the autocorrelation  $C^{BTW}(t, L)$ . I have verified (Fig. 3) that the exponential function  $f(t, L) \sim \exp(-\alpha_L t)$  better approximates not only the autocorrelation  $C^{BTW}(t, L)$  but also

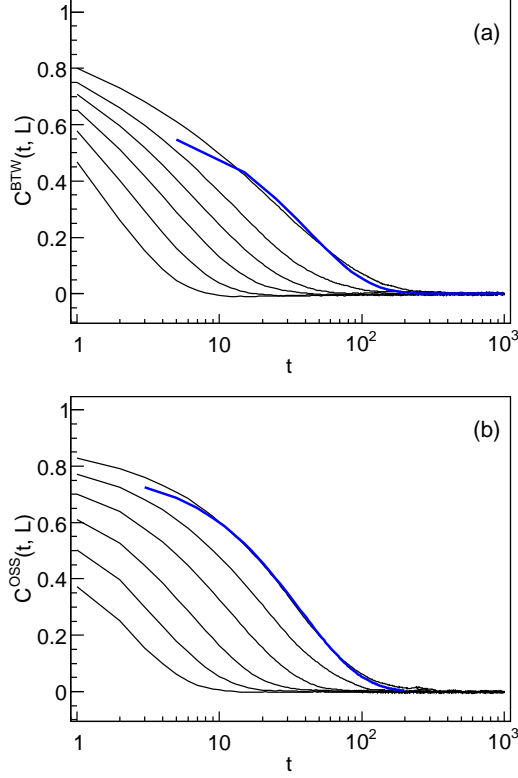


FIG. 3: (color online) Log-lin plots of autocorrelation functions  $C^{BTW}(t, L)$  and  $C^{OSS}(t, L)$  (threshold  $E_c^I = 4$ ) for lattices:  $L = 128, 256, 512, 1024, 2048$  and  $4096$  (from left to right). The autocorrelation functions  $C^X(t, L)$  for given lattice sizes  $L$  and for time  $t > 5$  are approximated by an exponential function  $C^X(t, L) \sim \exp(-\alpha_L t)$  (thick lines) where decay rates are: (a)  $\alpha_{4096}^{BTW} = 0.0244$  (BTW model) and (b)  $\alpha_{4096}^{OSS} = 0.027$  (OSS model).

$C^{OSS}(t, L)$ .

The autocorrelations  $C(t, L)$  from Eq. 3 are used to compute the time moments [11]:

$$\langle t^q \rangle_L = \sum_t C(t, L) t^q \sim L^{\sigma_c(q)}. \quad (4)$$

For lattice sizes  $L = 128 - 2048$ , threshold  $E_c^I = 4$  and for several values of  $q$ , the plots of  $\log \langle t^q \rangle$  vs.  $\log L$  (Fig. 4, inset) were used to determine the functions  $\sigma_c^{BTW}(q)$  and  $\sigma_c^{OSS}(q)$ . The plots  $\sigma_c^{BTW}(q)$  and  $\sigma_c^{OSS}(q)$  exhibit linear dependence for  $q$  in the range  $1.0 \leq q \leq 4.0$ . From these plots (Fig. 4) the parameters  $D_c^{BTW} = 1.06 \pm 0.05$ ,  $D_c^{OSS} = 1.09 \pm 0.05$ ,  $\tau_c^{BTW} \doteq 0$  and  $\tau_c^{OSS} \doteq 0$  were determined [11].

Stochastic process are often characterized by Hurst exponents [18]. Fluctuations  $F(t, L)$

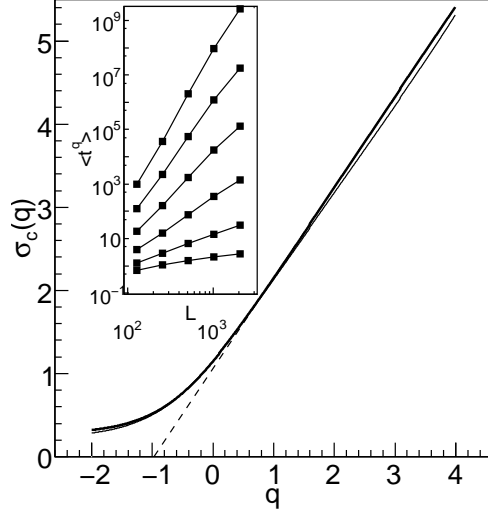


FIG. 4: The plots of  $\sigma_c(q)$  are approximated by the linear function  $\sigma_c(q) = p_1 q + p_0$ . For the BTW model (thin line) the parameters are  $p_1 = 1.06 \pm 0.05$ ,  $p_0 = 1.06 \pm 0.05$  and for the OSS model at threshold  $E_c^I = 4$  (thick line) the parameters are  $p_1 = 1.09 \pm 0.05$ , and  $p_0 = 1.06 \pm 0.05$  (this approximation is shown with dashed line). The inset shows log-log plots of  $\langle t^q \rangle$  vs.  $L$  for the OSS model and for the exponents  $q = -1, 0, 1, 2, 3$  and  $4$  (from bottom to top).

[11]:

$$F(t, L) = [\langle \Delta y(t)^2 \rangle_L - \langle \Delta y(t) \rangle_L^2]^{1/2}, \quad (5)$$

are used to determine Hurst exponents where  $y(t) = \sum_{k=1}^t s_k$  and  $\Delta y(t) = y(k+t) - y(k)$ . If fluctuations  $F(t, L)$  should scale as  $F(t, \infty) \sim t^H$  then  $H$  is the Hurst exponent [11]. Two exponents  $H^{BTW} = 0.89 \pm 0.02$  and  $H^{BTW} \doteq 1/2$  (Fig. 5) were determined for the BTW model and for times  $t < t_{max}^{BTW}$  and  $t > t_{max}^{BTW}$ . Similarly, the Hurst exponents  $H^{OSS} = 0.88 \pm 0.02$  and  $H^{OSS} = 0.610 \pm 0.001$  were determined for the OSS model (threshold  $E_c^I = 4$ ) and for times  $t < t_{max}^{OSS}$  and  $t > t_{max}^{OSS}$ . Fluctuations  $F(t, L)$  were also determined for the other thresholds  $8 \leq E_c^I \leq 256$  (Fig. 5). For all thresholds  $4 \leq E_c^I \leq 256$  of the OSS model two scaling regions of  $F(t, L)$  were identified in contrast to the fluctuation of the M model which exhibits the single scaling with the Hurst exponent  $H^M = 0.53 \pm 0.05$  (it is not shown in Fig. 5).

Moment analysis [9, 11, 12] was used to study scaling properties of both BTW and OSS models. A property  $x$  in the FSS system obeys the scaling given by Eq. 1. The  $q$  moments

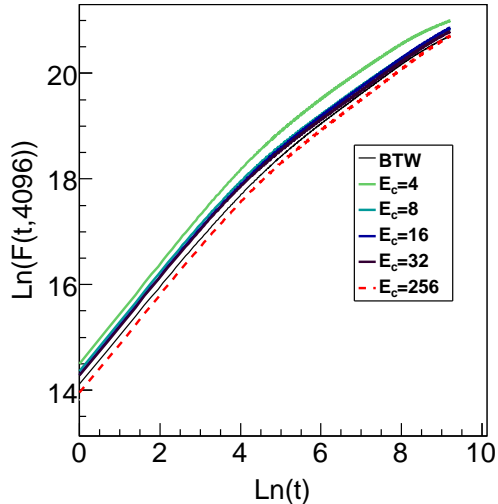


FIG. 5: (color online) The fluctuations  $F(t, L = 4096)$  of the BTW and OSS model with thresholds  $4 \leq E_c^I \leq 256$ . The Hurst exponents were determined for the threshold  $E_c^I = 4$ :  $H^{BTW} = 0.89 \pm 0.01$  and  $H^{OSS} = 0.88 \pm 0.01$ , the time  $1.0 < t < 50.0$ ,  $H^{BTW} = 0.503 \pm 0.001$  and  $H^{OSS} = 0.610 \pm 0.001$  for the time  $1000.0 < t < 10000.0$ .

of  $x$  are defined as

$$\langle x^q \rangle = \int_0^{x_{max}} x^q P(x, L) dx \sim L^{\sigma_x(q)}, \quad (6)$$

where  $\sigma_x(q) = (q + 1 - \tau_x)D_x$  and  $x_{max} \sim L^{D_x}$ . I calculated the moments only for avalanche size  $s$ . The plots  $\log\langle s^q \rangle$  versus  $\log L$  for approximately five hundred values of the exponent  $q$  were used to determine the functions  $\sigma_s^{BTW}(q)$  and  $\sigma_s^{OSS}(q)$  (Eq. 6). These plots scale precisely for the BTW model (Fig. 6(a)) and for the OSS model (threshold  $E_c^I = 4$ , Fig. 6(b)) for all exponents  $0.0 \leq q \leq 4.0$  and lattice sizes  $128 \leq L \leq 4096$ .

The results show that  $\sigma_s^{BTW}(1.0) = 2.03$  and  $\sigma_s^{OSS}(1.0) = 2.04$  for threshold  $E_c^I = 4$  (Fig. 7, inset), close to the expected value  $\sigma_s^{BTW}(1) \doteq 2.0$  [12, 16]. The function  $\sigma_s^{OSS}(q)$  grows faster than functions  $\sigma_s^{BTW}(q)$  and  $\sigma_s^M(q)$  (Fig. 7, inset) when the exponent  $q > 1.0$  increases. The function  $\partial\sigma_s^{OSS}(q)/\partial q$  increases with increasing  $q > 1.0$ . At  $q = 2.07$  it reaches the maximum  $D_s^{OSS}(2.07) = 3.17 \pm 0.01$  and for  $q > 2.07$  is almost constant or slowly decreases. For  $q = 4.0$ , the capacity dimensions are  $D_s^M(4) = 2.76$ ,  $D_s^{BTW}(4) = 2.88$  [13] and  $D_s^{OSS}(4) = 3.11 \pm 0.02$ . The functions  $\partial\sigma_s^{BTW}(q)/\partial q$  and  $\partial\sigma_s^{OSS}(q)/\partial q$  continuously increase when the exponent  $q$  increases in the range  $1.0 < q < 2.07$ . This fact is considered

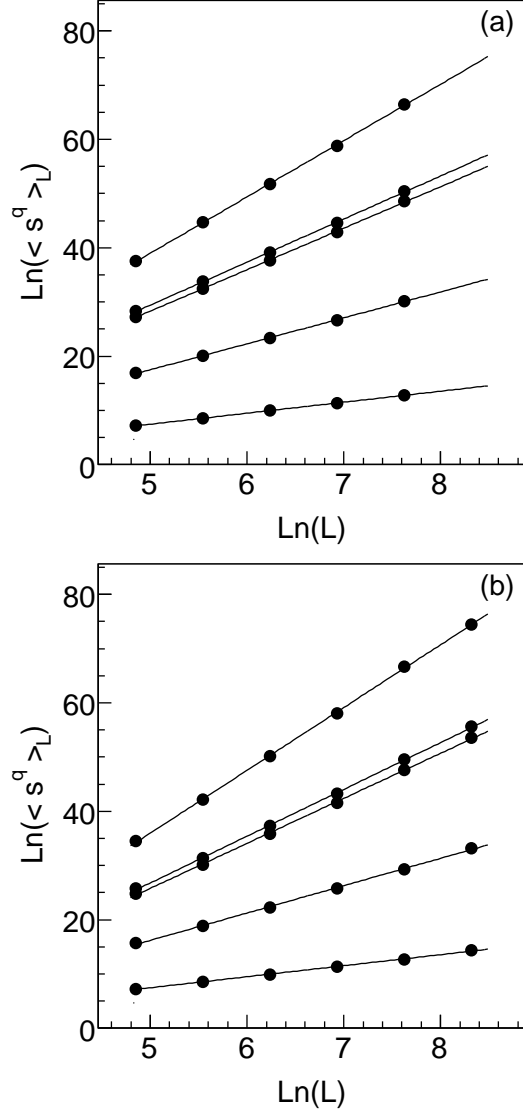


FIG. 6: Avalanche size moments  $\langle s^q \rangle_L$  at lattice size  $L$  versus lattice size  $L$  display scaling behaviour for wide range of exponents  $q$ . The results are shown for (a) the BTW model ( $128 \leq L \leq 2048$ ) and (b) the OSS model with threshold  $E_c^I = 4$  ( $128 \leq L \leq 4096$ ) whereas selected exponents  $q$  are  $q = 1.0, 2.0, 3.0, 3.1$  and  $4.0$  (from bottom to top).

to be a signature of multifractal scaling [9, 12]. The capacity dimension of the Manna model  $D_s^M(q)$  is constant for exponents  $q > 1.0$ :  $D_s^M(q) = 2.76 \pm 0.01$  [12, 13, 16], which is a typical property of the FSS models [12, 16].

Karmakar *et al.* [12] claimed that if local avalanche dynamics meets criterion of a precise relaxation balance, then the model must show the same behaviors as the BTW model. If we increase the threshold  $E_c^I > 4$  and we modify the relaxation rules to meet the criterion of

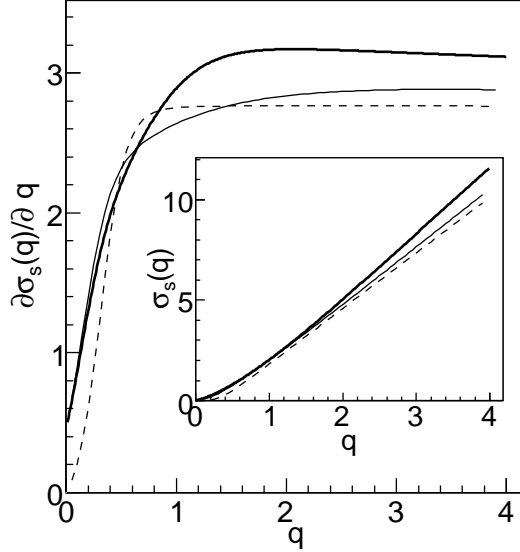


FIG. 7: Plots of  $\partial\sigma_s(q)/\partial q$  versus  $q$  for the M (dashed curves,  $128 \leq L \leq 2048$ ), BTW (thin line,  $128 \leq L \leq 2048$ ) and OSS models for the thresholds  $E_c^I = 4$  (thick solid,  $128 \leq L \leq 4096$ ). The inset shows plots  $\sigma_s(q)$  versus  $q$  for the M (dashed line,  $128 \leq L \leq 2048$ ), BTW (thin line,  $128 \leq L \leq 2048$ ) and OSS (thick solid,  $128 \leq L \leq 4096$ ) models.

the precise relaxation balance, then the model with all deterministic sites [19] has the same properties as the BTW model. In this model, for thresholds  $8 \leq E_c^I \leq 256$ , I introduced one stochastic site in each avalanche to compare the behaviors of the modified SOC model (see Sec. II) with the behaviors of the BTW model.

Autocorrelations  $C(t, L)$  Eq. 2 were determined for the OSS model with the thresholds  $4 \leq E_c \leq 256$ . Avalanches waves within avalanches are correlated (Fig. 8) for all thresholds because for the time  $t < t_{max}$  autocorrelations  $C(t, L)$  are greater than 0 ( $C(t, L) > 0$ ) and for the time  $t > t_{max}$  the autocorrelations approach the value  $C(t, L) \doteq 0.0$ .

Functions  $\partial\sigma_s^{OSS}(q)/\partial q$  of the OSS model for thresholds  $4 \leq E_c \leq 256$  and function  $\partial\sigma_s^{BTW}(q)/\partial q$  of the BTW model are shown in Fig. 9. The results show that  $\partial\sigma_s^{OSS}(q)/\partial q > \partial\sigma_s^{BTW}(q)/\partial q$  for thresholds  $4 \leq E_c \leq 256$  and for exponents  $1.0 \leq q \leq 4.0$ . A difference between functions  $\partial\sigma_s^{OSS}(q)/\partial q - \partial\sigma_s^{BTW}(q)/\partial q$  at given exponent  $q$  is observed to be higher than an expected experimental error [12].

Probability density functions  $P(s)$  of avalanche size  $s$  were determined for different lattice sizes  $L = 128, 512$  and  $4096$  (Fig. 10 (a)) and thresholds  $E_c^I = 4, 8$  and  $256$  (Fig. 10 (b)) to know the impact of the lattice size  $L$  or thresholds  $E_c^I$  on the probability density functions

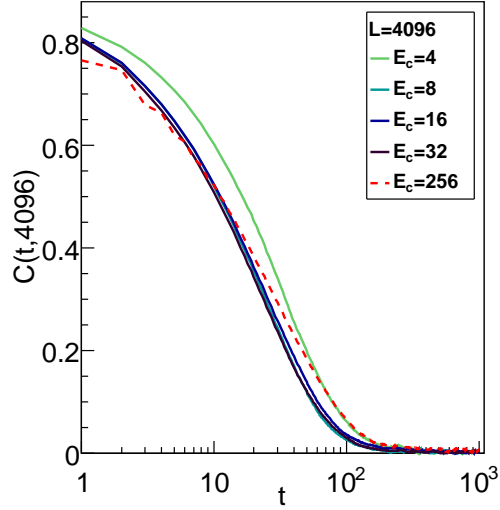


FIG. 8: (color online) Autocorrelations  $C(t, L = 4096)$  of the OSS model for thresholds  $4 \leq E_c^I \leq 256$ .

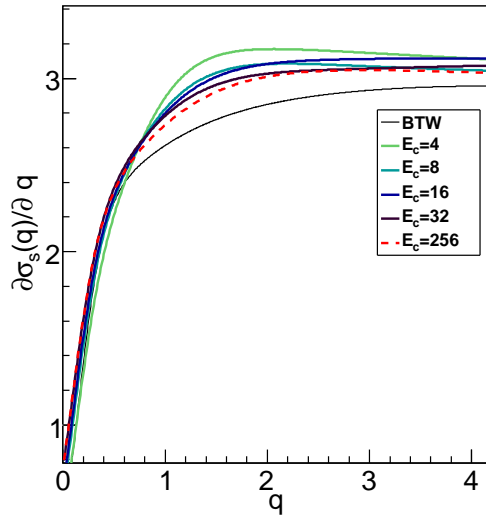


FIG. 9: (color online) The plots of  $\partial\sigma_s(q)/\partial q$  of the BTW and OSS ( $4 \leq E_c \leq 256$ ) models ( $128 \leq L \leq 4096$ ).

$P(s)$ . The probability density functions  $P(s)$  of the OSS model show small increases of their slopes for avalanches of size  $s < 10$ .

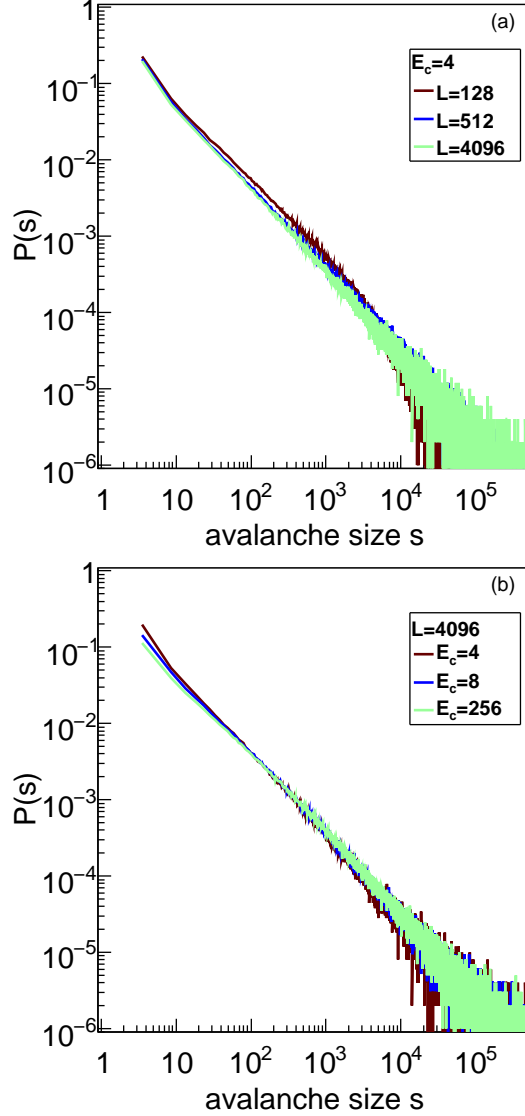


FIG. 10: (color online) Probability distribution functions  $P(s)$  of avalanche size  $s$  for (a) the constant threshold  $E_c = 4$  and increasing lattice size  $L = 128, 512$  and  $4096$  and for (b) the constant lattice size  $L = 4096$  and increasing thresholds  $E_c = 4, 8$  and  $256$ .

#### IV. DISCUSSION

The avalanche structures of the OSS model (Fig. 2) are similar to the shell-like structures of the BTW model[7, 9]. However, detailed analysis of these structures shows that the structures do not have the same properties as the structures of the BTW model. For example, we can see holes inside OSS structures (Fig. 2 (b)) which are not possible in the BTW model [12]. These holes support our classification of the OSS model as a model with

unbalanced relaxation rules [12].

Autocorrelations  $C(t, L)$  of the OSS model for thresholds  $4 \leq E_c^I \leq 256$  (Figs. 3(b) and 8) are  $C(t, L) > 0$  for times  $t_{max}$ . This is a consequence of correlated avalanche size waves within avalanche [2, 17]. Autocorrelations of the BTW model are the same as in the paper[11]. However, I cannot confirm that these autocorrelations are approximated by the power law approximation in Eq. 3. I have observed that an exponential function  $C(t, L) \sim \exp(-\alpha t)$  where  $\alpha$  is a decay rate, is a better approximation of the autocorrelations  $C(t, L)$  than the power law approximation Eq. 3. This finding is supported by the fact that time-moment analysis (Fig. 4) for the BTW and OSS models leads to the time exponents  $\tau^{BTW} \doteq 0$  and  $\tau^{OSS} \doteq 0$ . The reason for this discrepancy with the previous results [11] is not clear and additional study is necessary. On the other hand, the maximum number of waves scales as  $t_{max}^{BTW} \sim L$  and this result confirms the previous observation [11]. Similarly, for the OSS model  $t_{max}^{OSS} \sim L$  (Fig. 4).

The fluctuations  $F(t, L)$  and corresponding Hurst exponents  $H_1^{BTW}$  and  $H_2^{BTW}$  of the BTW model (Fig. 5) agree well with the previous results [11, 12]. Fluctuations  $F(t, L)$  of the OSS model for thresholds  $4 \leq E_c^I \leq 256$  have two scaling regions (Fig. 5) and corresponding Hurst exponents  $H_1^{OSS}$  and  $H_2^{OSS}$ . An existence of two scaling regions confirms the correlated avalanche size waves.

The moments of avalanche size Fig. 7 for the BTW and M models agree well with previous results [11, 12]. The plots  $\partial\sigma_s(q)/\partial q$  of the OSS model in Figs. 7 and 9, for thresholds  $4 \leq E_c^I \leq 256$  and exponents  $q > 1.0$ , are not constant as in the case of the M model. The increase of  $\partial\sigma_s(q)/\partial q$  for  $q > 1.0$  when the exponent  $q$  increases is considered for a signature of multifractal scaling [9, 11]. Based on the moment analysis (Figs. 7 and 9) for the thresholds  $4 \leq E_c^I \leq 256$  and previous conclusions [9, 11, 17], I claim that avalanche size distributions show multifractal scaling.

Probability density functions of avalanche size  $P(s)$  of the OSS model show a moderate increase of small avalanches  $s < 10$  for thresholds  $4 \leq E_c^I \leq 256$  (Fig. 10). I assume that these changes of probability density functions  $P(s)$  do not influence scaling of avalanche size moments (Fig. 6).

Holes in some avalanches (Fig. 2(b)) are characteristic for the models with unbalanced relaxation rules which exhibit uncorrelated avalanche waves [7, 12]. On the other hand, the existence of holes in the OSS model is not sign of uncorrelated waves because avalanche

size waves are correlated (see correlations  $C^{OSS}(t, L)$  (Fig. 3 (b) and 8) and fluctuations  $F^{OSS}(t, L)$  (Fig. 5)) exhibit two scaling regions.

Shell-like avalanche structures [7, 12], avalanche wave correlations  $C^{OSS}(t, L)$  [11, 12], avalanche wave fluctuations  $F^{OSS}(t, L)$  [11] and avalanche size moments  $\sigma_s^{OSS}(q)$  [11, 12] of the OSS model support the conclusion that the OSS model shows multifractal scaling for thresholds  $4 \leq E_c^I \leq 256$ . I can reproduce the plots  $\partial\sigma_s^{BTW}(q)/\partial q$  and  $\partial\sigma_s^{OSS}(q)/\partial q$  (Fig. 7) for thresholds  $4 \leq E_c^I \leq 256$ . Comparison of the functions  $\partial\sigma_s^{BTW}(q)/\partial q$  with the previous results of the BTW model and undirected model [12] shows that these functions collapse to a single function. I demonstrated that the OSS model shows multifractal scaling but the functions  $\partial\sigma_s^{OSS}(q)/\partial q$ , for thresholds  $4 \leq E_c^I \leq 256$ , are not identical with the function  $\partial\sigma_s^{BTW}(q)/\partial q$  of the BTW model (Figs. 7, 9). The differences between functions  $\partial\sigma_s^{BTW}(q)/\partial q$  and  $\partial\sigma_s^{OSS}(q)/\partial q$  at given exponent  $q$  are larger than the method error [12]. Based on these evidences, I conclude that OSS and BTW models belong to the multifractal universality class. However, the models do not have identical properties despite the fact that in the OSS model only one site in each avalanche undergoes stochastic relaxations as the M site.

## V. CONCLUSION

The OSS model has been developed to study properties of the inhomogeneous sand pile model [13] at very low densities of M sites [20]. Based on traditional classification schemes [12], one can expect that the model will belong to the M universality class. However, I have demonstrated that one stochastic M site in each avalanche is not enough to change multifractal scaling of the model to the FSS (Fig. 7). The OSS model is stochastic, *non-Abelian* with unbalanced relaxation rules [12], the classification schema implies that the model belongs to the M universality class. However, the OSS models exhibits correlated avalanche waves and multifractal scaling which is not allowed for the models in the M universality class. The OSS model exhibits multifractal scaling and the classification scheme implies that the model belongs to the BTW universality class, however the model is stochastic, non-Abelian, and has an unbalanced relaxation rule [12], thus it cannot belong to the BTW class. I think that it could be more convenient to consider multifractal or FSS scaling as a main criterion for model classification to solve this paradox. Then the models which show multifractal scaling

(Fig. 7, BTW and OSS models) despite the fact that they are not identical (see Sec. III) could belong to the multifractal universality class. Models that show FSS scaling Eq. 1 (M model) could belong to the FSS universality class. I have analyzed another SOC model where the results support this classification scheme [19].

Thanks to Alex Read for reading the manuscript and for discussion. Computer simulations were carried out with NorduGrid community resources and in the KnowARC project. This work was supported by the Slovak Research and Development Agency under contract No. RP EU-0006-06.

- 
- [1] P. Bak, C. Tang, and K. Wiesenfeld, Phys. Rev. Lett. **59**, 381 (1997); Phys. Rev. A **38**, 364 (1988).
  - [2] S. S. Manna, J. Phys. A **24**, L363 (1991).
  - [3] D. Dhar, Physica A **263**, 4 (1999); Physica A **369**, 29 (2006).
  - [4] D. Dhar, Physica A **270**, 69 (1999).
  - [5] L. Pietronero, A. Vespignani, and S. Zapperi, Phys. Rev. Lett. **72**, 1690 (1994); A. Vespignani, S. Zapperi and L. Pietronero, Phys. Rev. E **51**, 1711 (1995).
  - [6] H. E. Stanley, A. Vespignani, and S. Zapperi, Phys. Rev. E **59**, R12 (1999).
  - [7] A. Ben-Hur and O. Bihami, Phys. Rev. E **53**, R1317 (1996).
  - [8] S. Lbeck and K. Usadel, Phys. Rev. E **55**, 4095 (1997).
  - [9] C. Tebaldi, M. de Menech, and A. L. Stella, Phys. Rev. Lett. **83**, 3952 (1999).
  - [10] E. V. Ivashkevich, D. V. Ktitarov, and V. B. Priezhev, Physica A **209**, 347 (1994).
  - [11] M. De Menech and A. L. Stella, Phys. Rev. E **62**, R4528 (2000).
  - [12] R. Karmakar, S. S. Manna, and A. L. Stella, Phys. Rev. Lett. **94**, 088002 (2006).
  - [13] J. Černk, Phys. Rev. E **73**, 066125 (2006).
  - [14] O. Biham, E. Milshstein, and O. Malcai, Phys. Rev. E **63**, 061309 (2001).
  - [15] D. Dhar, Phys. Rev. Lett. **64**, 1613 (1990).
  - [16] S.B. Santra, S. R. Chanu, and D. Deb, Phys. Rev. E **75**, 041122 (2007).
  - [17] A. L. Stella and M. De Menech, Physica A **295**, 101 (2001).
  - [18] Benoit B. Mandelbrot, *The fractal geometry of nature* (W. E. Freeman and Company, New

York, 1983).

[19] J. Černík, arXiv:0908.0318v1 [cond-mat.stat-mech].

[20] J. Černák and J. Bobot, manuscript is being prepared.